



UNIVERSITÀ
DEGLI STUDI
DI PADOVA

Università degli Studi di Padova

Padua Research Archive - Institutional Repository

A computational assessment of the aerodynamic performance of a tilted Darrieus wind turbine

Original Citation:

Availability:

This version is available at: 11577/3181485 since: 2016-02-18T16:09:51Z

Publisher:

Elsevier

Published version:

DOI: 10.1016/j.jweia.2015.07.005

Terms of use:

Open Access

This article is made available under terms and conditions applicable to Open Access Guidelines, as described at <http://www.unipd.it/download/file/fid/55401> (Italian only)

(Article begins on next page)



A Computational Assessment of the Aerodynamic Performance of a Tilted Darrieus Wind Turbine

Gabriele Bedon*, Stefano De Betta, Ernesto Benini

Department of Industrial Engineering, University of Padua, Via Venezia 1, 35131 Padua, Italy

Abstract

The aerodynamic performance of a Darrieus wind turbine operating with the rotation axis tilted with respect to the free-stream wind speed is investigated in this paper. An Unsteady Reynolds Averaged Navier Stokes (URANS) Computational Fluid Dynamics (CFD) model is proposed in order to provide wind turbine manufacturers with a reliable simulation tool to forecast the power conversion characteristics of vertical axis wind turbine prototypes that operate in tilted conditions. The outputs of the model are compared against experimental performance of a non-tilted rotor corrected to the standard sea level conditions. Two different tilted configurations are studied (i.e., a tilt angle of 10° and 20°), and the aerodynamic performance are presented in terms of the mechanical power production and the power coefficient. A sensible decrease in the power production is observed for increasing tilt angles. Comprehensive physical interpretations of the results are provided, considering also the predictions of a methodology based on semi-empirical methods.

Keywords: Vertical Axis Wind Turbines, Tilted Darrieus, 3D URANS CFD, Offshore Wind Turbines

1. Introduction

During the last decade, wind energy has experienced a cubic growth [1] due to the increasing awareness for the need of a renewable energy source that could provide humanity with a solution to overcome the actual fossil fuel dependency. In this regard, the ongoing research on wind turbine technology development has resulted in new concepts that improve the production and reduce the cost of energy.

Similarly to horizontal axis wind turbines, which are now being constructed in offshore locations in order to exploit the observed higher power density and increase its size without incurring Not In My Back Yard (NIMBY) issues, Vertical Axis Wind Turbines (VAWTs) are also recently object of research activities in order to prove the feasibility of offshore configurations with sensibly increased size. Among the different VAWTs types, Darrieus wind turbines are the most interesting due to the higher efficiencies and reduced loads compared to other configurations.

*Corresponding author, email: gabriele.bedon@dii.unipd.it, tel. +39 049 8276770

11 Experimental tests on Darrieus turbines with increasing size were performed in the recent past by the most
12 important research centers. Literature provides the aerodynamic performance for rotors with characteristic lengths of
13 2 meters [2], 5 meters [3], 17 meters [4, 5], 34 meters [6], 37 meters [7, 8], and 96 meters [9, 10]. These tests provided
14 the most reliable experimental results for the performance of these machines and enable wind turbine designers to
15 perform validation studies of their simulation methods over the widest range of Darrieus configurations [11].

16 Based on the experience of onshore installations, a variety of research projects aimed to deploy Darrieus wind
17 turbines in offshore environments. Differently from horizontal axis wind turbines, whose installations generally
18 include foundation technologies that constraint the turbine movement (e.g., monopile, gravity base, tripod base, and
19 jacket structures) [12, 13, 14], a floating concept is being analysed for vertical axis wind turbines, which would allow
20 its installation in deeper waters [15].

21 Nowadays two main projects are being conducted by the main institutions of the offshore vertical axis wind turbine
22 research. The *Inflow* project [16] aims at demonstrating the cost competitiveness and provide an industrial prototype
23 of a helical Darrieus turbine that might be installed on a semi-submersible floater support structure. A 26 MW wind
24 farm is designed as target to complete the first phase of its industrialization process, with 13 turbines to be built and
25 installed, based on the background experience developed during onshore and offshore tests. The *Deepwind* project
26 [17, 18, 19] proposed an equivalent floating offshore wind turbine concept, which consists of a long axis that rotates in
27 the water, with a vertical axis Troposkien rotor placed on the top, a generator located at the bottom of the rotor and a
28 sea-bed support structure system [20]. In this system, the vertical axis rotor is targeted to reach a power production of
29 5 MW. The rotor swept area needed to obtain such power production leads the project researchers to adopt a modified
30 Troposkien shape rotor [21] with a characteristic length of about 130 m.

31 The aerodynamic performance for these type of rotors was estimated by considering the wind turbine as perfectly
32 vertical (i.e., orthogonal) to the free-stream wind speed, despite the rotor, due to the floating support structure, will
33 mostly operate in a tilted configuration. This approximation is usually made in most conventional semi-empirical
34 models used to simulate the aerodynamic performance of vertical axis wind turbines e.g., the Blade-Element
35 Momentum theory [22, 23, 24] or Vortex models [25]. Tilted conditions are generally treated by reducing the
36 performance of a tilted rotor by considering only the projection of the free-stream wind speed on the rotor plane
37 [26, 27].

38 The purpose of the present work is to provide a modeling approach to forecast the aerodynamic performance of a
39 tilted Darrieus rotor with a Troposkien shape. The limitations of conventional semi-empirical methods are overcome
40 by considering an unsteady three-dimensional URANS $k-\omega$ SST CFD model, whose validation against experimental
41 data for a 2 meter rotor [2] is presented in this paper. This size is adopted, beside for the availability of experimental

42 data, to compare the numerical predictions with the 2-meter Deepwind demonstrator [28], which is operating in these
 43 particular conditions. Results, however, have general validity, since the Troposkien shape is simply scaled for turbines
 44 characterized by larger dimensions.

45 2. Experimental Data

46 The experimental data provided by Sheldahl [2] of a 2-meter wind turbine are considered in the validation of
 47 the URANS-based simulations. The rotor is 2-meter high with a maximum radius of 0.98 m. The blade shape is
 48 straight-circular-straight (SCS): this is considered a good approximation of the Troposkien architecture [21] but it is
 49 cheaper to manufacture. The physical characteristics of the wind turbine are reported in Table 1, while a picture of
 50 the wind turbine installation at the Sandia test site is shown in Figure 1.

H [m]	2
R [m]	0.98
N_B [-]	3
Blade profile	NACA 0012
Blade shape	Straight-circular-straight (SCS)
c [mm]	58.77

Table 1. Main geometrical features of the baseline rotor configuration.

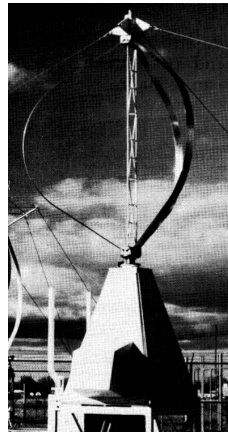


Figure 1. Sandia 2-meter Darrieus wind turbine installation (from: [2]).

51 Open-field and wind tunnel tests were conducted considering two rotational speeds, 400 *rpm* and 460 *rpm*. The
 52 two tests provide results in good agreement with respect to the tip speed ratio. The comparison with the URANS-based
 53 simulations is therefore performed considering only the experimental data from the wind tunnel test at a rotational

54 speed of 400 rpm. The technical report [29] indicates that the chord Reynolds number, defined as:

$$Re_c = \frac{\omega R c}{\nu} \quad (1)$$

55 was kept constant for this specific test at a value of $1.54 \cdot 10^5$.

56 The cinematic viscosity for the test can be evaluated and results to be $\nu = 1.566 \cdot 10^{-5} \text{ m}^2/\text{s}$. This value is different
57 from the common reference value at the standard sea level, which will be also adopted in the CFD simulation. In fact,
58 considering an air density of $\rho = 1.225 \text{ kg/m}^3$ and a dynamic viscosity of $\mu = 1.789 \cdot 10^{-5} \text{ kg m/s}$ [30], the cinematic
59 viscosity at the standard sea level is $\nu = 1.460 \cdot 10^{-5} \text{ m}^2/\text{s}$.

60 Retaining the original chord Reynolds number, a corrected rotational speed can be calculated from the standard
61 cinematic viscosity, which results to be 371.09 rpm. The tip speed ratios are also corrected and a shifted performance
62 curve is obtained, which is reported in Figure 2. This curve, which represents the rotor efficiency at the standard sea
63 level, is considered in the following CFD validation.

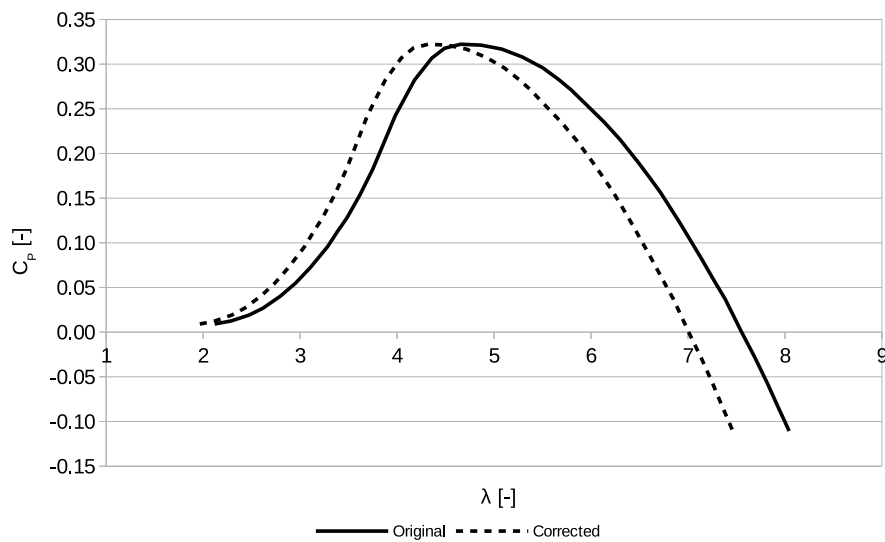


Figure 2. Original and cinematic viscosity corrected performance of the Sandia 2-meter rotor from the wind tunnel test.

64 3. CFD Validation

65 The URANS CFD simulations are conducted employing the commercial software Ansys Fluent 14.5 [31]. The
66 adopted turbulence model is the $k - \omega$ SST. This model was chosen due to its accuracy and reliability to predict
67 complex aerodynamics under a wide of fluid flow conditions, including cases with adverse pressure gradients acting
68 on two-dimensional airfoils [32, 33]. The introduction of a blending function, which combines the Wilcox $k - \omega$ model

69 and the standard $k - \epsilon$, ensures that the model equations behave appropriately in both the near-wall and far-field zones.
 70 In the near-wall boundary, the k equation of the $k - \omega$ SST model is treated in the same way as the k equation of the
 71 $k - \epsilon$, which relies on the enhanced wall treatment approach. This means that for spatial discretizations concentrated
 72 towards the wall, which are defined by values of the dimensionless wall distance y^+ [31] close or lower than the unity
 73 (hereinafter referred as "fine meshes"), the appropriate low-Reynolds-number boundary condition is applied, while
 74 the wall function approach is used for meshes characterized by y^+ values larger than unity, hence properly taking into
 75 consideration the inner layers of the boundary layer. [31]. The simulation is set to unsteady with a timestep equal to
 76 the time needed for the rotor to perform an azimuthal rotation of 1 degree. The spatial and temporal discretizations
 77 are performed considering second order schemes. The time-step converges when the scaled residual values [34] fell
 78 below 10^{-5} , since lower values would not lead to sensible difference in the estimations [35]. The rotor torque varies in
 79 every time step due to the simulation unsteadiness. The final average torque value T is estimated when the simulation
 80 is considered as periodic, i.e. when the difference between average torque values in sequential rotational periods is
 81 lower than 1%. This value is adopted to compute the power production P and the power coefficient C_P , in formulas:

$$C_P = \frac{P}{0.5 \cdot \rho \cdot A \cdot v^3} = \frac{T \cdot \omega}{0.5 \cdot \rho \cdot A \cdot v^3} \quad (2)$$

82 The Sandia turbine is modelled as a three-blade rotor with the physical characteristics reported in Table 1. The
 83 three blades are connected with each other on the top and the bottom of the rotor through the introduction of two
 84 truncated cones. The central shaft is disregarded in the simulation due to the lack of information about its geometry [2],
 85 and due to the limited effect of its wake, which affects only the downwind production [32, 35, 36]. This approximation
 86 moreover helps to reduce the computational complexity.

87 The simulation domain is rectangular with an allowance axial and vertical distances respectively of 20 m and 3 m.
 88 This shape is selected to reproduce a virtual wind tunnel with neglectable blockage effects: the adopted distances,
 89 largely greater than 10 times the chord length, were chosen to minimize the influence of the boundary walls. The
 90 domain is divided into two sub-domains, *gallery* and *cylinder*, to define different spatial discretizations and the rotor
 91 motion in the *cylinder* domain. The two domains are shown in Figure 3, where the size and the boundary conditions
 92 are also indicated. The validation case with the 2-meter rotor presents a perfect symmetry between the top and the
 93 bottom rotor halves, since a uniform wind speed is imposed at the velocity-inlet. Thus only half of the rotor is
 94 simulated, placing a symmetry boundary condition at the rotor middle plane. A *velocity inlet* boundary is imposed at
 95 the inlet, considering a uniform wind speed. The outlet is considered as a *pressure outlet*, with a gauge pressure of
 96 0 Pa. Since the simulation aims to reproduce the wind tunnel tests, a low level of turbulence is set both at the inlet and
 97 the outlet: the turbulence intensity was 0.1% and the turbulent viscosity ratio was 10, as suggested by the software

98 User Guide [37]. The blades are considered as *no-slip walls*. Since additional details are not provided by the reference
 99 paper from Sheldahl [2], walls are considered smooth with a roughness height of 0 m.

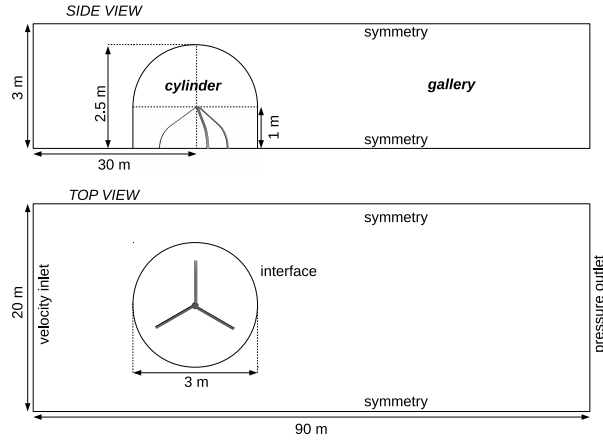


Figure 3. Scheme of the computational domains with boundary conditions and sizes.

100 A sensitivity analysis is conducted to study the most important mesh parameters. A hexahedral mesh extrusion is
 101 created over the rotor blades, in order to simulate the blade's boundary layer. The first element height is estimated by
 102 imposing the maximum y^+ value in all the rotor **near-wall** cells to be lower than 1, an approximated value which is
 103 reported to maximize the reliability of the turbulence model [31]. The number of mesh extrusion steps and the growth
 104 rate were object of investigation, since these parameters strongly influence the total number of discretized elements,
 105 while other parameters are kept constant **as** reported in Table 2.

Number of elements on the blade airfoil	244
Number of elements on the blade length	300
Leading edge spacing [mm]	0.15
Trailing edge spacing [mm]	0.20
First layer height [mm]	0.011
Cylinder wall mean element size [mm]	85
Gallery wall mean element size [mm]	350
Volume mesh growth rate	1.15

Table 2. Geometrical parameters of the baseline mesh.

106 Two different configurations for the boundary layer extrusions were considered:

- 107 (i) 27 steps with a growth rate of 1.15;
 108 (ii) 15 steps, 10 layers with a growth rate of 1.15 and 5 layers with a growth rate of 1.5.

109 **Simulations are conducted considering tip speed ratios between 2 and 6 and the results are reported in Figure**

110 4. **The peak power coefficients and their tip speed ratios obtained with both mesh configurations are close to the**

111 experimental data. A good agreement is also registered with both mesh configurations at high tip speed ratios, whereas
 112 for low tip speed ratios the mesh with 15 steps is overpredicting the performance. The difference is, however, very
 113 limited.

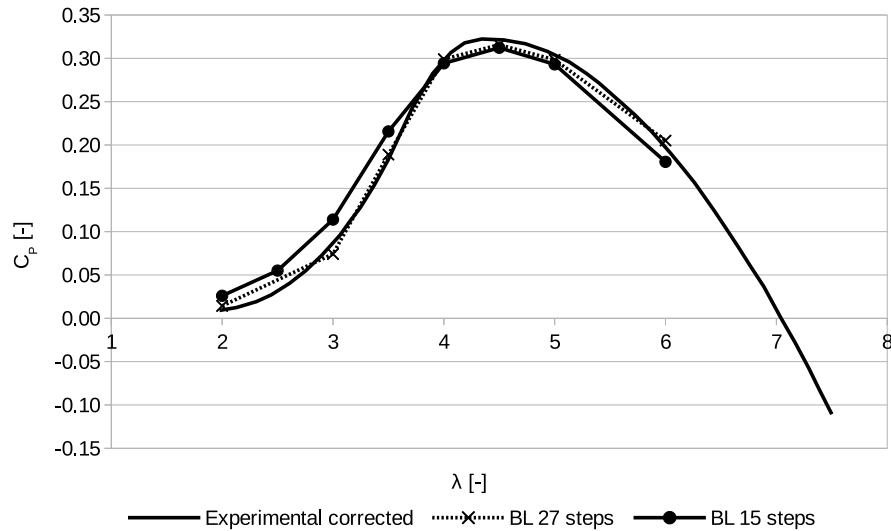


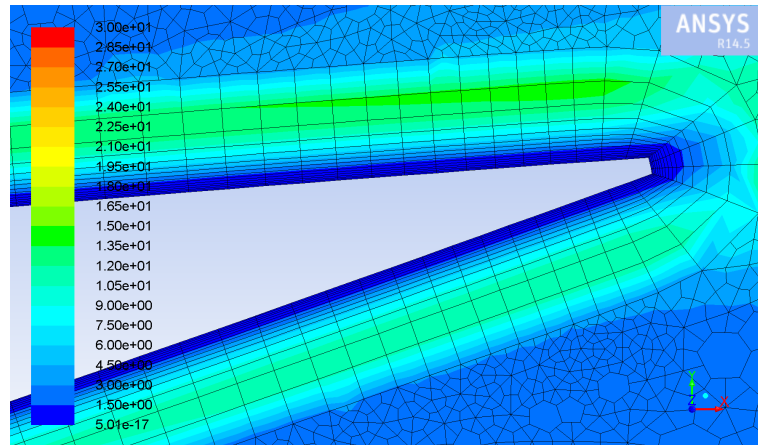
Figure 4. Simulation results with two different configurations for the boundary layer extrusion.

114 Moreover, the mesh with 15 steps is capable to capture completely the boundary layer when the airfoil is not
 115 stalling. The turbulent viscosity ratio experiences, in fact, a large rise and dissipation confined in the prism layer, as
 116 can be seen in Figures 5(a) and 5(b) for two azimuthal positions. This is not observed in Figure 5(c) for a different
 117 azimuthal position, since the airfoil stalls and the boundary layer is detached.

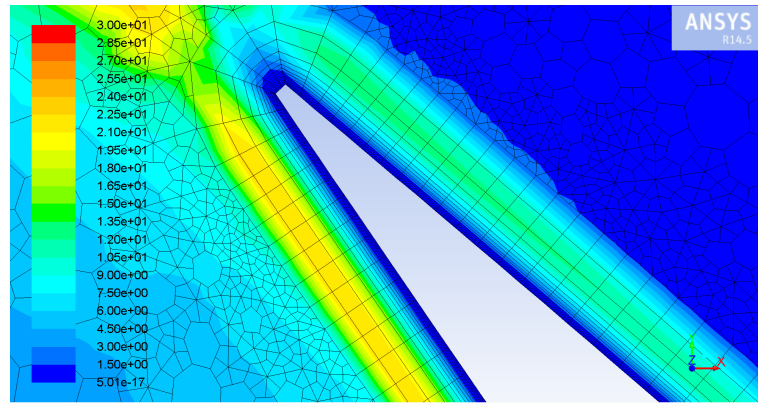
118 On the other hand, the simulation of a tilted Darrieus turbine requires two times the number of discretized
 119 elements, since the the blade airfoils from the upper and lower rotor halves would interact with the fluid at different
 120 angles of attack. The number of elements required for the configuration with 27 step extrusion is not compatible with
 121 the available computational power, since it exceeds the 64 GB RAM requirements. Therefore the configuration with
 122 15 step extrusion is selected, showed in Figure 6.

123 A sensitivity analysis is also conducted with respect to the number of elements on the base airfoils of the blade
 124 on a single operative condition, $\lambda = 4$. The simulation results are reported in Table 3. The CFD simulation with the
 125 higher number of elements is closer to the experimental result. On the other hand, a small difference is registered in the
 126 power coefficient values estimated by CFD simulations and, due to the limitation in the RAM usage, the configuration
 127 with 244 elements on the profile is adopted.

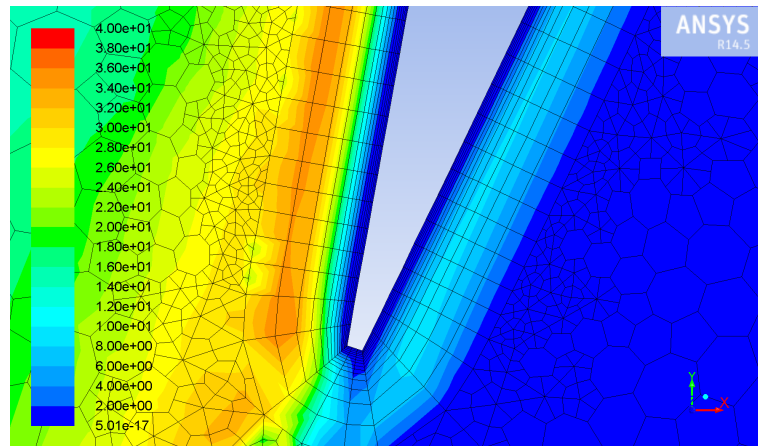
128 The mesh is characterized by 13.8 millions of cells and the unsteady simulation requires about 60 GB of RAM
 129 memory. A computer equipped with a 8-core Intel Xeon E5-2650 2.00 Ghz takes about 10 minutes to complete a



(a) $\beta = 12^\circ$



(b) $\beta = 132^\circ$



(c) $\beta = 252^\circ$

Figure 5. Turbulent viscosity ratio near the airfoil at different azimuthal positions, $\lambda = 4.5$.

130 single time-step, whereas the final torque value is obtained after the simulation of 2500 time-steps on average.

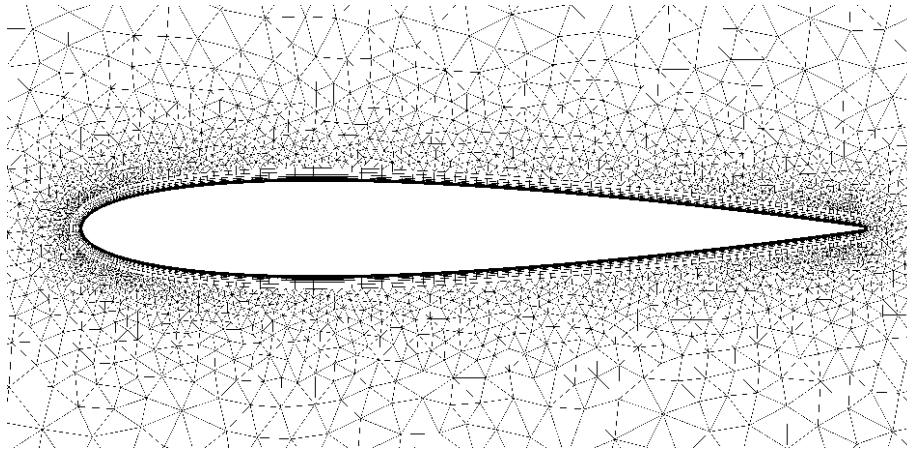


Figure 6. Airfoil mesh with 15 step boundary layer extrusion.

Configuration	Power Coefficient [-]
Experimental corrected	0.300
CFD, 244 elements on profile	0.294
CFD, 364 elements on profile	0.304

Table 3. Simulation results for $\lambda = 4$ with two number of elements on the profile of the blade airfoil.

131 4. Results and Discussion

132 The domain for the tilted Darrieus simulation is created by rotating the *cylinder* domain around the rotor virtual
 133 central point with a defined angle. The *gallery* domain is reconstructed afterwards, as showed in Figure 7. The rotor
 134 rotation and the torque calculation are specified considering the new tilted axis.

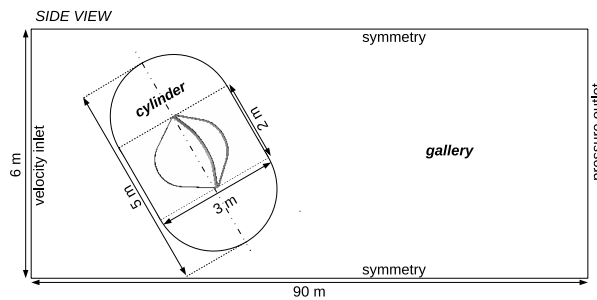
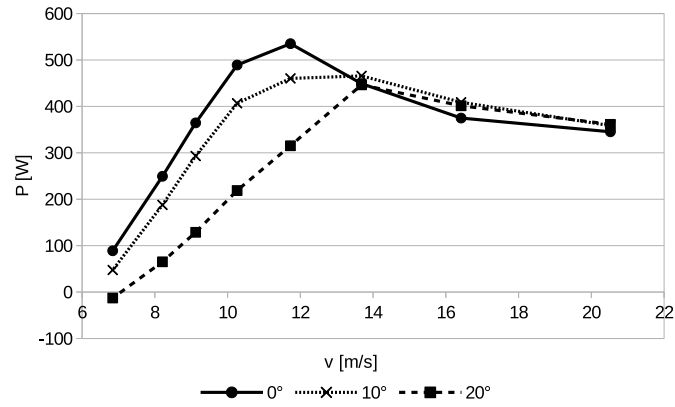


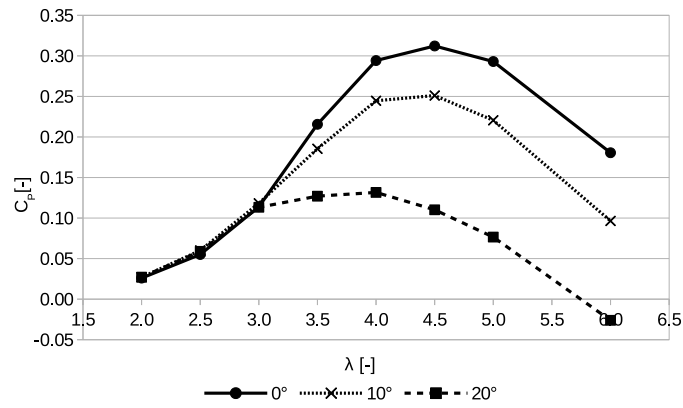
Figure 7. Scheme of the computational domains for the tilted configuration with boundary conditions and sizes, no to scale.

135 During offshore operations, the rotor blades should not impact the water during rotation. The tilt angle is therefore
 136 expected, and should be forced, not to exceed the angle at the Troposkien root, which is about 30° . Simulations
 137 are therefore conducted considering two tilted configurations, with a tilt angle equals to 10° and 20° . The power
 138 production P with respect to the free-stream wind speed v and the power coefficient C_p with respect to the tip speed
 139 ratio λ for the two tilted configurations are reported in Figure 8, whereas the peak power coefficient values, the relative

tip speed ratios and their variations with respect to the vertical configuration are reported in Table 4.



(a) Power production with respect to the wind speed.



(b) Power coefficient with respect to the tip speed ratio.

Figure 8. Aerodynamic performance for the two tilted configurations obtained with the URANS CFD simulations.

Configuration	$\lambda_{\max C_P}$ [-]	$\max C_P$ [-]	$\Delta\lambda_{\max C_P}$ [-]	ΔC_P [-]
0°	4.5	0.3122		
10°	4.5	0.2511	0.00%	-19.57%
20°	4.0	0.1316	-11.11%	-57.83%

Table 4. Peak power coefficient values, relative tip speed ratios and variations with respect to the vertical configuration.

The comparison between the performance of the non-tilted and tilted rotors can be analysed by considering the rotor behaviour before and after a particular operative point characterized by the operative condition of $\lambda = 3$, approximately equal to $v = 14\text{m/s}$. The tilted rotor operating at high tip speed ratios, corresponding to lower wind speeds, i.e. lower angles of attack, is experiencing an expected decrease in the power production due to the unfavorable effective wind direction. As reported by Johnson [38], the aerodynamic forces in a yawed wing can be estimated, for small angles of attack, by considering the two-dimensional aerodynamic coefficients but with different wind speeds:

147 the lift and the drag force should be computed, respectively, using the projected and the free-stream wind speeds, the
 148 former lower than the latter. Consequently, the reduction in the lift force with respect to the drag force will lead to a
 149 reduction in the rotor torque.

150 As stated before, this trend is generally considered in the semi-empirical analysis by reducing the inflow wind
 151 speed, approximately by the cosine of the tilt angle [26, 27]. Figure 9 shows a comparison between the performance
 152 estimated by the URANS CFD approach and those obtained by interpolating the simulation results with a reduced
 153 inflow wind speed calculated as:

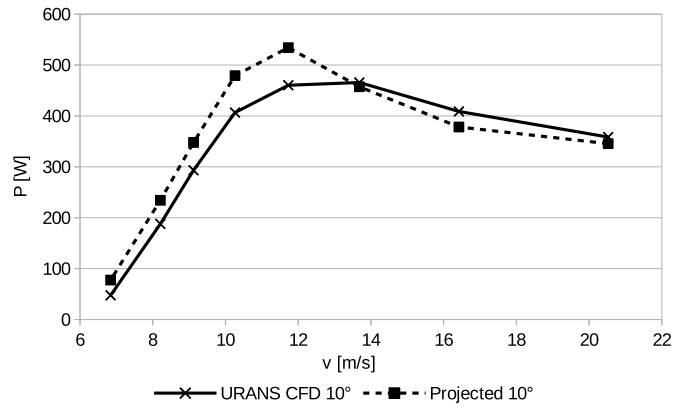
$$v = v_{\infty} \cdot \cos \theta \quad (3)$$

154 The accuracy of the prediction obtained by projecting the wind speed is very limited since performance are
 155 over-predicted with respect to the URANS CFD simulations for the lower wind speeds. Whereas a shifting trend
 156 of the production curve can be still observed, as the peak production is reduced and moved to higher wind speeds,
 157 a more accurate model to be adopted in semi-empirical methods is needed to predict this aerodynamic effect in the
 158 tilted rotors.

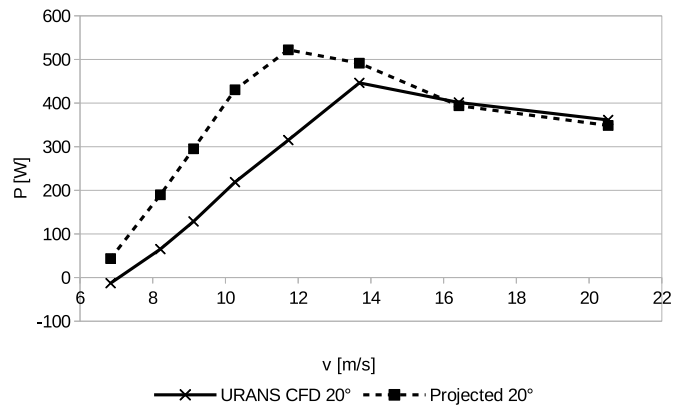
159 The tilted rotor performance at **tip speed ratios** higher than $\lambda = 3$ are instead comparable to the vertical rotor
 160 configuration. The power coefficient values are super-imposed whereas a small increase in the power performance
 161 is observed. The reason behind this behaviour can be found in the profile aerodynamics. In the operative conditions
 162 above the peak power production, in fact, the rotor is operating at stalled conditions with large angles of attack. In
 163 these conditions, small variations in the angle of attack, due to the rotor tilt, lead to limited variations around the zero
 164 value of the tangential force coefficient C_t [22], defined as:

$$C_t = C_L \sin \alpha - C_D \cos \alpha \quad (4)$$

165 The coefficient values with respect to different angles of attack derived from the experimental NACA 0012
 166 coefficient database developed by Jacobs [39] and extended by Bedon et al. [11] are plotted in Figure 10 for two
 167 Reynolds numbers typical of these operative conditions. Variations in the rotor torque, calculated from the average C_t
 168 value, are therefore limited too. This explanation can be also confirmed by observing that the performance obtained
 169 by projecting the wind speed on the rotor plane, which involves a small change in the angle of attack, are in good
 170 agreement with those from URANS CFD simulations. Moreover, since the three-dimensional nature of the separated
 171 flow due to the boundary layer detachment influences the whole blade aerodynamics [40], no relevant differences
 172 between the tilted and vertical configurations should be expected.



(a) Tilt angle of 10° .



(b) Tilt angle of 20° .

Figure 9. Performance of the two tilted configurations, estimated by URANS CFD simulations and interpolation of the curve with a reduced wind speed.

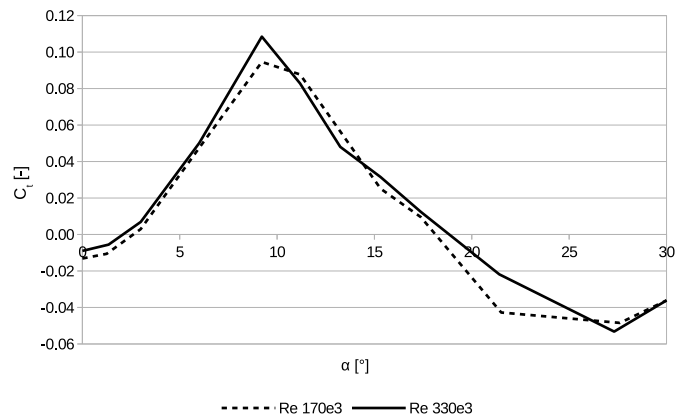


Figure 10. Tangential force coefficient C_t with respect to the angle of attack for two operational Reynolds numbers.

173 5. Conclusions and Future Works

174 This work presented a CFD-based study of the aerodynamic performance of a Darrieus wind turbine operating
175 under tilted conditions.

176 As a first step, an URANS approach based on the $k-\omega$ SST turbulence model was developed to predict the unsteady
177 aerodynamics of the Darrieus rotor. A sensitivity analysis was conducted to determine the proper value of the most
178 important parameters of the finite-volume domain discretization. Acceptable agreement between the experimental
179 and the numerical results in non-tilted conditions was found, enabling the use of the model for the analysis of the
180 tilted configurations.

181 Two tilt angles were considered due to the operative restrictions linked to the Troposkien shape: 10° and 20° .
182 The performance of the vertical-axis wind turbine was reported in terms of the power production and the power
183 coefficient. As expected, a reduced performance was observed with increasing tilt angle. However, two different
184 trends were observed as a function of the tip speed ratio. For high tip speed ratios, a strong decrease in the power
185 coefficient was observed. This performance attenuation is linked to the yawed airfoil theory. A comparison between
186 the URANS estimations and the results obtained by simply projecting the wind speed along the rotor plane highlighted
187 the limitation of the second approach, which is unable to account for the three-dimensional effects due to the tilted
188 inflow. At low tip speed ratios, the tilted rotor performance was comparable with the perfectly vertical configuration.
189 This behaviour is linked to the stalled operative conditions of the rotor, since the tangential coefficient C_t is little
190 varying with a variation of the angle of attack. Estimations based on the wind speed projection, which relies on the
191 same hypothesis, are in fact accurate.

192 These computational predictions represent the first attempt to provide an estimation of the aerodynamic
193 performance in tilted configurations, which are often experienced in offshore conditions. A validation with
194 experimental results would provide a final confirmation on the accuracy of the CFD approach and would allow to
195 perform a deeper analysis of the Darrieus aerodynamics in these unconventional operative conditions. Moreover,
196 corrections for semi-empirical models could be developed in order to overcome the actual limitations, leading to more
197 complete theories which could be adopted in much comprehensive analyses.

198 **Nomenclature**

$A [m^2]$	Rotor swept area
$c [m]$	Airfoil chord
$C_D [-]$	Airfoil drag coefficient
$C_L [-]$	Airfoil lift coefficient
$C_P [-]$	Rotor power coefficient
$C_t [-]$	Tangential force coefficients
$H [m]$	Rotor height
$N_B [-]$	Number of blades
$P [W]$	Power produced by the turbine
$R [m]$	Rotor maximum radius
$Re_c [-]$	Chord Reynolds number
$T [Nm]$	Final average torque value
$v [m/s]$	Reference wind velocity
$v_\infty [m/s]$	Free-stream wind velocity
$y^+ [-]$	Dimensionless wall distance
$\alpha [^\circ]$	Airfoil angle of attack
$\beta [^\circ]$	Airfoil azimuthal position
$\lambda [-]$	Tip speed ratio
$\mu [kg\ m/s]$	Dynamic viscosity
$\nu [m^2/s]$	Cinematic viscosity
$\rho [kg/m^3]$	Air density
$\theta [^\circ]$	Rotor tilt angle
$\omega [rad/s]$	Rotor rotational speed

199 **References**

- 200 [1] American Wind Energy Association, U.S. Wind Industry Annual Market Report 2014, Tech. rep., American Wind Energy Association,
 201 Washington, D.C., U.S.A. (2014).
- 202 [2] R. E. Sheldahl, Comparison of field and wind tunnel Darrieus wind turbine data, Tech. rep., Sandia National Laboratories Report
 203 SAND80-2469 (1981).
 204 URL <http://infoserve.sandia.gov/sand.doc/1980/802469.pdf>

- 205 [3] R. E. Sheldahl, P. C. Klimas, L. V. Feltz, Aerodynamic performance of a 5-metre-diameter Darrieus turbine with extruded aluminum
206 NACA-0015 blades, Tech. rep., Sandia National Laboratories Report SAND80-0179 (1980).
207 URL <http://www.wrapwind.com/download/800179.pdf>
- 208 [4] M. H. Worstell, Aerodynamic performance of the 17-metre-diameter Darrieus wind turbine, Tech. rep., Sandia National Laboratories Report
209 SAND78-1737 (1979).
210 URL <http://prod.sandia.gov/techlib/access-control.cgi/1978/781737.pdf> <http://www.estonia.ca/koit/Kool/L?put??/Muud>
211 [materjalid/Sandia/Teisej?rgulised/Sandia_781737.pdf](http://www.estonia.ca/koit/Kool/L?put??/Muudmaterjalid/Sandia/Teisej?rgulised/Sandia_781737.pdf)
- 212 [5] M. H. Worstell, Aerodynamic performance of the 17-m-diameter Darrieus wind turbine in the three-bladed configuration: An addendum,
213 Tech. rep., Sandia National Laboratories Report SAND79-175 (1982).
214 URL <http://adsabs.harvard.edu/abs/1980STIN...8026857W>
- 215 [6] T. D. Ashwill, Measured data for the Sandia 34-meter vertical axis wind turbine, Tech. rep., Sandia National Laboratories Report
216 SAND91-2228 (1992).
217 URL http://infoserve.sandia.gov/sand_doc/1991/912228.pdf
- 218 [7] R. J. Templin, R. S. Rangi, Vertical-axis wind turbine development in Canada, IEE Proceedings A Physical Science, Measurement and
219 Instrumentation, Management and Education, Reviews 130 (9) (1983) 555. doi:10.1049/ip-a-1.1983.0085.
220 URL <http://digital-library.theiet.org/content/journals/10.1049/ip-a-1.1983.0085>
- 221 [8] R. D. McConnell, J. H. Vansant, M. Fortin, B. Piché, An experimental 200 kW vertical axis wind turbine for the Magdalen Islands, in: 11th
222 Intersociety Energy Conversion Engineering Conference, American Institute of Chemical Engineers, New York, 1976, pp. 1798–1802.
223 URL <http://adsabs.harvard.edu/abs/1976iece.conf.1798M>
- 224 [9] J. Déry, Éole, aérogénérateur à axe vertical de 4 MW à Capchat, Québec, Canada, in: Intersol Eighty Five: Proceedings of the Ninth Biennial
225 Congress of the International Solar Energy Society, 1986, pp. 2030–2034.
- 226 [10] H. Benjannetm, Structural Design for 4 MW VAWTG - Project Eole, in: Intersol Eighty Five: Proceedings of the Ninth Biennial Congress of
227 the International Solar Energy Society, 1986, pp. 2047–2051.
- 228 [11] G. Bedon, E. G. A. Antonini, S. De Betta, M. Raciti Castelli, E. Benini, Evaluation of the Different Aerodynamic Databases for Vertical Axis
229 Wind Turbine Simulations, Renewable & Sustainable Energy Reviews 40 (2014) 386–399.
- 230 [12] C. N. Elkinton, Offshore Wind Farm Layout Optimization, Ph.D. thesis, University of Massachusetts (2007).
231 URL <http://books.google.com/books?id=oJ8qKheYDQkC&pgis=1>
- 232 [13] P. Gardner, A. Garrad, P. Jamieson, H. Snodin, G. Nicholls, A. Tindal, Volume 1: Technology., in: Wind Energy - The Facts, European Wind
233 Energy Association, Brussels, Belgium, 2004.
- 234 [14] H. Svensson, Design of foundations for wind turbines, M.Sc. Thesis - Lund University.
- 235 [15] M. Raciti Castelli, S. De Betta, E. Benini, Preliminary Evaluation of Feasibility for Wind Energy Production on Offshore Extraction Platforms,
236 World Academy of Science, Engineering and Technology 6 (11) (2012) 1873–1878.
- 237 [16] <http://www.inflow-fp7.eu/>, accessed on February 2015.
- 238 [17] L. Vita, Offshore Floating Vertical Axis Wind Turbines with Rotating Platform, Risø-phd-80(en), Danmarks Tekniske Universitet (2011).
- 239 [18] U. Schmidt Paulsen, L. Vita, H. Aagård Madsen, J. H. Hattel, E. Ritchie, K. M. Leban, P. A. Berthelsen, S. Carstensen, 1st DeepWind 5 MW
240 baseline design, Energy Procedia 24 (2012) 27–35.
- 241 [19] U. Schmidt Paulsen, H. Aagård Madsen, J. H. Hattel, I. Baran, P. Hørlyck Nielsen, Design Optimization of a 5 MW Floating Offshore
242 Vertical-axis Wind Turbine, Energy Procedia 35 (2013) 22–32.
243 URL <http://www.sciencedirect.com/science/article/pii/S1876610213012411>

- 244 [20] <http://www.deepwind.eu/The-DeepWind-Project>, accessed on February 2015.
- 245 [21] G. E. Reis, B. F. Blackwell, Practical approximations to a troposkien by straight-line and circular-arc segments, Tech. rep., Sandia National
246 Laboratories Report SAND74-0100 (1975).
247 URL http://www.osti.gov/energycitations/product.biblio.jsp?osti_id=5115217
- 248 [22] J. H. Strickland, The Darrieus Turbine: A performance prediction model using multiple streamtubes, Tech. rep., Sandia National Laboratories
249 Report SAND75-0431 (1975).
250 URL <http://scholar.google.com/scholar?hl=en&btnG=Search&q=intitle:The+Darrieus+Turbine:+A+performance+prediction+model+us>
- 251 [23] I. Paraschivoiu, Double-multiple streamtube model for Darrieus in turbines, in: Wind Turbine Dynamics, Nasa Conference Publication 2185,
252 Cleveland, Ohio, USA, 1981, pp. 19–25.
253 URL <http://onlinelibrary.wiley.com/doi/10.1002/cbdv.200490137/abstract> <http://adsabs.harvard.edu/abs/1981wtd...nasa...19P>
- 254 [24] I. Paraschivoiu, F. Delclaux, Double multiple streamtube model with recent improvements, Journal of Energy 7 (3) (1983) 250–255.
255 URL <http://adsabs.harvard.edu/abs/1983JEner...7...250P>
- 256 [25] J. H. Strickland, B. T. Webster, T. Nguyen, A Vortex Model of the Darrieus Turbine: An Analytical and Experimental Study, Journal of Fluids
257 Engineering 101 (4).
258 URL <http://www.csa.com/partners/viewrecord.php?requester=gs&collection=TRD&recid=A8018620AH>
- 259 [26] A. Bianchini, G. Ferrara, L. Ferrari, S. Magnani, An Improved Model for the Performance Estimation of an H-Darrieus Wind Turbine in
260 Skewed Flow ACRONYMS, Wind Energy 36 (6) (2012) 667–686. doi:10.1260/0309-524X.36.6.667.
- 261 [27] K. Wang, M. Otto Laver Hansen, T. Moan, Model improvements for evaluating the effect of tower tilting on the aerodynamics of a vertical
262 axis wind turbine, Wind Energy 18 (January 2015) (2015) 91–110. doi:10.1002/we.
263 URL <http://onlinelibrary.wiley.com/doi/10.1002/we.1608/full>
- 264 [28] U. Schmidt Paulsen, T. Friis Pedersen, H. Aagård Madsen, K. Enevoldsen, P. Hørlyck Nielsen, J. H. Hattel, L. Zannel, L. Battisti, A. Brighenti,
265 M. Lacaze, V. Lim, J. W. Heinen, P. A. Berthelsen, S. Carstensen, E.-J. De Ridder, G. van Bussel, G. Tescione, Deepwind - An Innovative
266 Wind Turbine Concept for Offshore, in: EWEA 2011 Conference, 2011.
267 URL http://proceedings.ewea.org/annual2011/allfiles2/1269_EWEA2011presentation.pdf
- 268 [29] B. F. Blackwell, R. E. Sheldahl, L. V. Feltz, Wind tunnel performance data for the Darrieus wind turbine with NACA 0012 blades, Tech. rep.,
269 Sandia National Laboratories Report SAND76-013 (1976).
270 URL http://www.osti.gov/energycitations/product.biblio.jsp?osti_id=7269797
- 271 [30] B. W. McCormick, Aerodynamics, aeronautics and flight mechanics, 1994.
272 URL <http://as.wiley.com/WileyCDA/WileyTitle/productCd-0471575062.html>
- 273 [31] Ansys Inc., ANSYS FLUENT 14.5 Theory Guide, Canonsburg, PA, U.S.A., 2012.
- 274 [32] M. Raciti Castelli, G. Ardizzon, L. Battisti, E. Benini, G. Pavesi, Modeling Strategy and Numerical Validation for a Darrieus Vertical Axis
275 Micro-Wind Turbine, in: ASME 2010 International Mechanical Engineering Congress & Exposition IMECE2010-39548, Vancouver, British
276 Columbia (Canada), 2010.
277 URL <http://link.aip.org/link/abstract/ASMECP/v2010/i44441/p409/s1>
- 278 [33] F. Balduzzi, A. Bianchini, R. Maleci, G. Ferrara, L. Ferrari, Blade Design Criteria to Compensate the Flow Curvature Effects in H-Darrieus
279 Wind Turbines, Journal of Turbomachinery 137 (January) (2015) 1–10. doi:10.1115/1.4028245.
- 280 [34] Ansys Inc., ANSYS FLUENT 14.5 User's Guide, Canonsburg, PA, U.S.A., 2012.
- 281 [35] M. Raciti Castelli, A. Englaro, E. Benini, The Darrieus wind turbine: Proposal for a new performance prediction model based on CFD,
282 Energy 36 (8) (2011) 4919–4934. doi:10.1016/j.energy.2011.05.036.

283 URL <http://linkinghub.elsevier.com/retrieve/pii/S0360544211003616>

284 [36] M. Raciti Castelli, E. Benini, Effect of blade inclination angle on a Darrieus wind turbine, *Journal of Turbomachinery* 134 (2012)
285 031016–1–10.

286 URL <http://cat.inist.fr/?aModele=afficheN&cpsidt=25783928>

287 [37] Ansys Inc., ANSYS FLUENT 14.0 Theory Guide, Canonsburg, PA, U.S.A., 2011.

288 URL <http://scholar.google.com/scholar?hl=en&btnG=Search&q=intitle:ANSYS+FLUENT+Theory+Guide#1>

289 [38] W. Johnson, *Helicopter theory*, Dover Publications, 1980.

290 [39] E. N. Jacobs, A. Sherman, Airfoil section characteristics as affected by variations of the Reynolds number, Tech. rep., National Advisory
291 Committee for Aeronautics 586 (1937).

292 URL <http://aerade.cranfield.ac.uk/ara/1937/naca-report-586.pdf>

293 [40] J. Katz, Large-Scale Vortex-Lattice Model for the Locally Separated Flow over Wings, *American Institute of Aeronautics and Astronautics*
294 *Journal* 20 (12) (1982) 1640–1646.